ADVANCED FUNCTIONAL MATERIALS
www.afm-journal.de

Controlled Assembly of Poly(3-hexylthiophene): Managing the Disorder to Order Transition on the Nano- through Meso-Scales

*Dalsu Choi, Mincheol Chang, and Elsa Reichmanis**

Self-assembly of conjugated organic semiconductors into ordered, larger scale entities is a critical process to achieve efficient charge transport at the nano- through macro-scales, and various methodologies aimed at enhancing molecular ordering have been introduced. However, mechanistic understanding is limited. Here, a mechanistic elucidation of poly(3-hexylthiophene) (P3HT) molecular self-assembly is proposed based on experimental demonstration of controlled, solution-based P3HT self-assembly into rod-like polycrystalline nanostructures. The synergistic combination of nonsolvent addition and ultrasonication facilitates rod-like P3HT nanostructure formation in solution. Importantly, through sequential application of both treatments, nanostructure length can be easily modulated, and the assembly process is shown to follow a simple 2-step crystallization model, which depends upon nucleation followed by growth. Through arrays of experimental results, the validity of 2-step crystallization is confirmed and is proposed as a comprehensive platform to understand self-assembly processes of conjugated polymers into larger, ordered mesoscale entities.

1. Introduction

As strong candidates expected to enable practical applications in low-cost, flexible electronics, solution processable conjugated organic semiconducting materials have garnered much attention over the past decade. However, the inherently inferior charge carrier transport performance of organic semiconductors has led to a multitude of efforts focused on enhancing their transport properties.[1–4] These efforts have largely concentrated on the design and synthesis of alternative structures.[5–7] More recently, attention has turned to improving electronic performance via design and control of solution processing techniques. Methods focused on inducing ordering/crystallization of conjugated materials have effected significant performance improvements and are gaining traction due to their simplicity.[8–12] However, to date, most research related to crystallization of organic materials through solution processing methods has been confined to conjugated small molecules, which are more easily crystallized than polymeric alternatives.[13–15] While recent reports have presented processing methods to induce semiconducting polymer ordering,[16,17] inquiries into underlying mechanisms are limited, even though discernment of the self-assembly process is critically important.

In this paper, we systematically interpret and elicit control of the regio-regular poly(3-hexylthiophene) (P3HT) self-assembly process based on a 2-step crystallization model consisting of nucleation and growth steps. Starting from the demonstration of controlled P3HT molecular assembly into polycrystalline rod-like P3HT nanostructures with varied length, it is shown that the synergistic combination of ultrasonic irradiation and nonsolvent addition[18,19] leads to molecular self-assembly of P3HT into rod-like polycrystalline mesoscale architectures through simple 2-step crystallization principles. Though commonplace in the crystallization community,[20–23] 2-step crystallization has yet to be introduced to analyze conjugated polymer ordering into nanostructured assemblies. Application of 2-step crystallization principles may provide a comprehensive platform for analysis and discussion of conjugated polymer self-assembly into polycrystalline moieties that have favorable charge transport characteristics.

Adventitious control of self-assembled P3HT nanostructures effects notable improvement in P3HT charge carrier mobility values up to 0.103 ± 0.009 cm^2 V^{-1} s^{-1}, versus 0.025 ± 0.007 cm^2 V^{-1} s^{-1} for untreated samples were obtained. Through careful analysis of X-ray diffraction, UV–vis, and atomic force microcopy (AFM) morphological data, the important interplay between molecular level interactions and long-range order for effective macroscale charge carrier transport is articulated.

2. Results and Discussion

The process used to induce controlled P3HT self-assembly into nanorod structures is depicted in **Figure 1**. Chloroform and

D. Choi, Dr. M. Chang, Prof. E. Reichmanis
School of Chemical and Biomolecular Engineering
Georgia Institute of Technology
Atlanta, GA 30332, USA
E-mail: elsa.reichmanis@chbe.gatech.edu
Prof. E. Reichmanis
School of Chemistry and Biochemistry
Georgia Institute of Technology
Atlanta, GA 30332, USA
Prof. E. Reichmanis
School of Materials Science and Engineering
Georgia Institute of Technology
Atlanta, GA 30332, USA

DOI: 10.1002/adfm.201403708

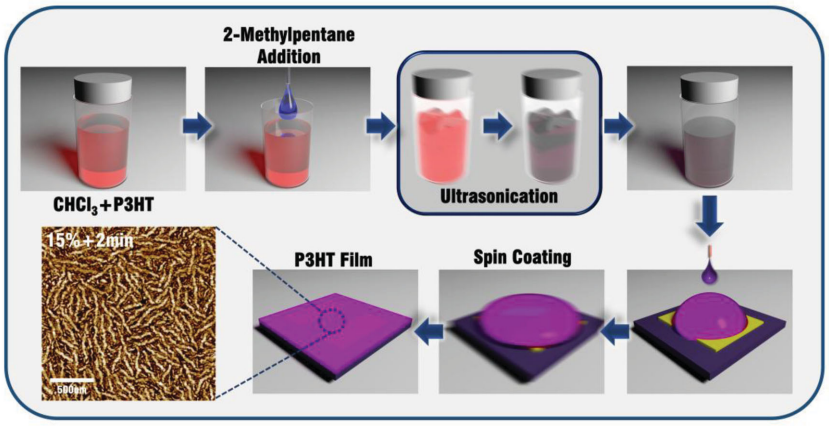

Figure 1. A schematic illustration of P3HT nanorod preparation through a combined ultrasonication/nonsolvent addition approach.

2-methylpentane were carefully chosen as the solvent and nonsolvent, respectively: their boiling points are similar (2-methylpentane, bp: 61 °C; chloroform, bp: 62 °C) and the two solvents do not significantly interact (e.g., hydrogen bonding) with each other. Thus, 2-methylpentane addition alters P3HT solubility, but has no impact on overall solvent volatility, one factor known to impact P3HT self-assembly during film formation.[24]

First, known amounts of 2-methylpentane were added to a P3HT/chloroform solution. This sequence facilitated selective control of solution solubility. After addition of poor solvent, the resultant P3HT solution was mediated by ultrasonic irradiation using a common bath type ultrasonicator. Ultrasonication is known to induce P3HT self-assembly with no change in molecular structure.[18,25] Finally, P3HT thin films were fabricated from the corresponding solutions via spin coating. As discerned from atomic force microscopy (AFM) phase images (**Figure 2**a), this step-wise methodology effected P3HT self-assembly into rod-like nanostructures whose dimensions could be modulated by varying the proportion of nonsolvent. For a fixed sonication time, solvent composition regulated final P3HT nanorod dimensions. Upon addition of 0–15 vol% 2-methylpentane, nanorod length was significantly elongated from ≈140 to ≈360 nm, while further increases in the proportion of nonsolvent led to drastic shortening of the assemblies.

As discerned from bottom gate, bottom contact organic field effect transistor (OFET) studies, P3HT charge carrier mobility increased gradually as a function of nanorod length. Devices fabricated from ultrasonicated P3HT solution with 15 vol% 2-methylpentane affords the longest P3HT nanorod assemblies and exhibited the highest average mobility, 0.103 $cm^2\ V^{-1}\ s^{-1}$, a value that is notably higher than that obtained from pristine P3HT films which are not subject to the additional treatments (Figure 2b). As nanorod length increased, mobility increased steeply. Presumably, films composed of a significant number of short assemblies leads to an increased number of boundaries between the more crystalline nanorods and amorphous-like matrix which serves to increase points of resistance impeding efficient charge transport.[26–28]

Grazing incidence X-ray diffraction (GIXRD) results provide insight into nanorod crystallite packing (**Figure 3**a,b). The full width half max (FWHM) of the (100) peak corresponding to lamellar packing of P3HT chains was analyzed, and the average crystallite size was calculated using the Scherrer equation.[29] Previous studies reported that pristine P3HT films are amorphous and show no (100) peak development,[18,30] and thus, the P3HT (100) FWHM is representative of crystallite size, where crystallites are presumed to consist of polymer nanorods. Significantly, crystallite size followed a trend similar to that of nanorod length; for up to 15 vol% 2-methylpentane where nanorod length was observed to increase, crystallite size also increased. Further increases in nonsolvent concentration led to a decrease in grain size, accompanied by an observed decrease in nanorod length. Given the direct correlation between nanorod length and thin film crystallinity, it is extrapolated that the polymer nanorod assemblies are crystalline features, whereby crystallite size is proportional to nanorod length.

From UV–vis spectroscopic data (Figure 3c), the absorption band near 620 nm became more prominent, while that at about 550 nm representing the π–π^* transition underwent a bathochromic shift as a function of 2-methylpentane volume fraction, indicative of enhanced intra- and intermolecular interactions among P3HT chains.[31–34] The spectra continued to evolve with increased 2-methylpentane volume fraction up to 40 vol%,where the system comprised very short P3HT nanorod-like structures. The data suggest that very short structures fabricated from 2 min ultrasonicated solutions containing 30 and 40 vol% 2-mehtylpentane exhibit stronger intra- and inter-molecular interactions than much longer P3HT nanorods assembled in 15 vol% 2-methylpentane solutions with 2 min ultrasonication (Figure 3d).

While the UV–vis spectroscopic results suggest that the P3HT thin films prepared from ultrasonicated solutions having a high volume fraction of nonsolvent enjoy stronger molecular scale interactions, those interactions alone do not guarantee assembly of the nanostructures into longer, ordered, mesoscale constructs necessary for effective macroscale charge carrier transport. Coupled with electronic performance, GIXRD and UV–vis analysis underscores the importance of optimal nanostructure growth conditions. Within individual small mesoscale structures fabricated in ultrasonicated, high nonsolvent content solutions, charge carrier transport may well be more effective due to stronger molecular-scale interactions than those found in the longer nanorod assemblies.[35–37] However, macroscale charge carrier mobility is significantly higher when the films comprise longer nanorods with somewhat weaker molecular level interactions. Unambiguously, long-range order plays a significant role in defining semiconducting polymer transport characteristics, and is perhaps more important than molecular level interactions for efficient macroscopic charge carrier transport.

The influence of molecular level interactions on charge carrier transport properties should not however, be disregarded. **Figure 4**a demonstrates that nanostructures with similar or

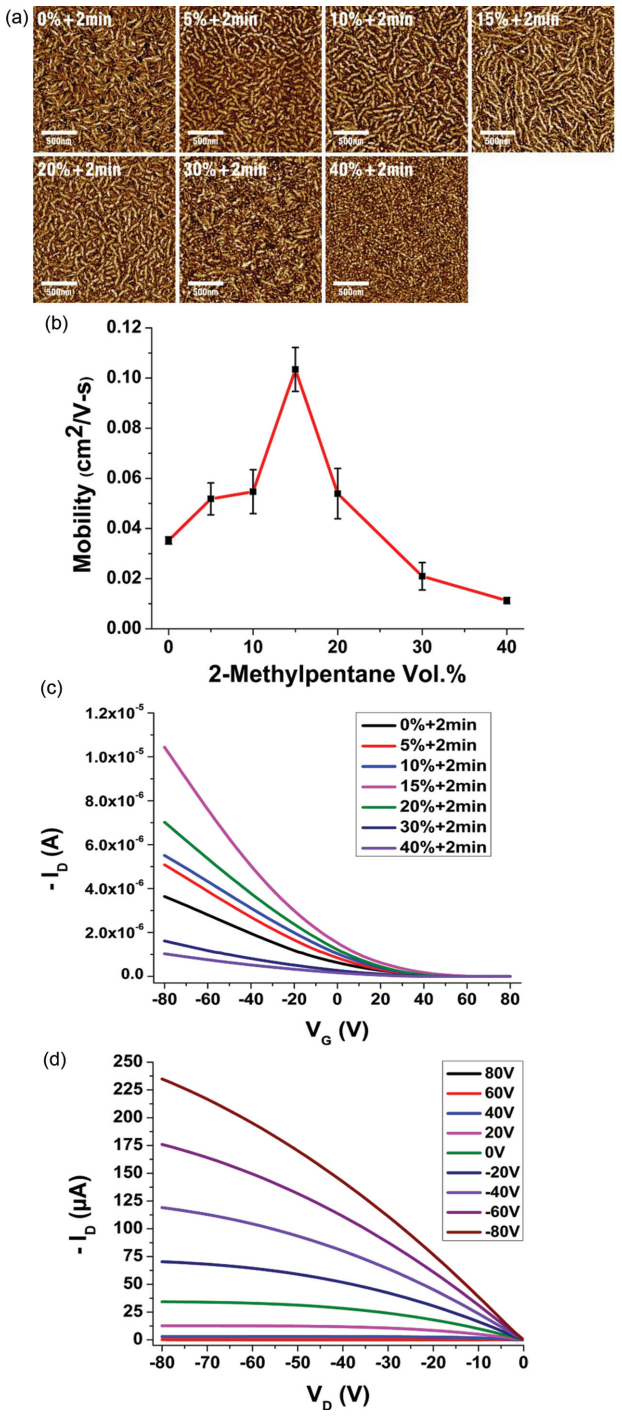

Figure 2. a) Tapping mode AFM phase images of P3HT films obtained by spin coating choloroform-P3HT solutions with varying proportions of nonsolvent (2-methylpentane) followed by ultrasonication for 2 min. b) Average field-effect mobilities of P3HT thin films spin coated from chloroform-P3HT solution with corresponding proportion of 2-methylpentane followed by 2 min of ultrasonication. Mobilities were calculated in the linear regime of operation with $V_{DS} = -3$ V. c) Transfer characteristics of OFET devices fabricated with corresponding P3HT solution. d) Representative output characteristic curve of OFET devices fabricated with chloroform-P3HT solution treated with 15 vol% 2-methylpentane and 2 min ultrasonication.

slightly longer lengths can be created by modulating system solubility. P3HT nanostructures prepared through addition of 15 vol% 2-methylpentane coupled with 2 min ultrasonication (Figure 2a) and nanostructures assembled via 20% 2-methylpentane addition alone (Figure 4a) have almost identical length, thus suggesting a similar degree of charge transport resistance through boundaries between more crystalline nanorods and amorphous domains for both films. However, the hole mobility exhibited by devices fabricated from solutions prepared via addition of 20% 2-methylpentane was only 0.042 ± 0.005 cm^2 V^{-1} s^{-1}, a value less than half that observed for films prepared by the synergistic solvent modulation/ultrasonication approach.

The large mobility gap observed for P3HT films comprising nanostructures with similar dimensions most likely derives from differences in their respective molecular level interactions. The intensity of the absorption band near 620 nm, indicative of the extent of molecular level interactions, is significantly more intense in the case where both solubility modulation and ultrasonication were employed. It is deduced that once P3HT self-assembles into nanorods with sufficient length to allow for long-range order, molecular level interactions within individual mesoscale entities play a role in macroscale charge transport. However, strong molecular level interactions in and of themselves, in the absence of concomitant long-range order, cannot support efficient macroscopic charge transport. While both long-range order and molecular level interactions are required for optimal charge carrier transport at the device level, each factor plays an important role, and both can be extrinsically influenced or tempered by a range of process variables for optimized transport. Here, solution characteristics and postdissolution treatments such as ultrasonication were used to demonstrate the important relationship/tradeoff.

To define optimum solution characteristics for explicit control of P3HT nanostructure dimensions, a mechanistical description of the self-assembly process is required. A 2-step crystallization model consisting of nucleation and growth steps is adopted to elucidate P3HT self-assembly. While established in other areas,[20–23] application of this model provides new insight into the crux of P3HT ordering/crystallization processes and significantly, similar processes that are generically operational in conjugated polymer systems.

The essential driving force for crystallization from solution relies on the degree of supersaturation.[20] In the metastable state, where a solution is moderately supersaturated (**Figure 5**a,b), crystal growth is initiated from available nucleation sites. Within this metastable zone, crystal growth is favored over formation of nucleation sites. From the perspective of P3HT, polymer molecules would be consumed in crystal growth, which emanates from existing nucleation sites. In contrast to behavior within the metastable state, if the solution becomes further supersaturated, it enters an unstable regime (Figure 5c), where nucleation dominates crystal growth, and most of the excess solute becomes subject to spontaneous nucleation.[20,38–40]

Using the nucleation and growth crystallization model, Figure 5d depicts four generic scenarios for P3HT nanorod assembly. Systems A and B have the identical number of P3HT chains available for ordering, though System B is comprised

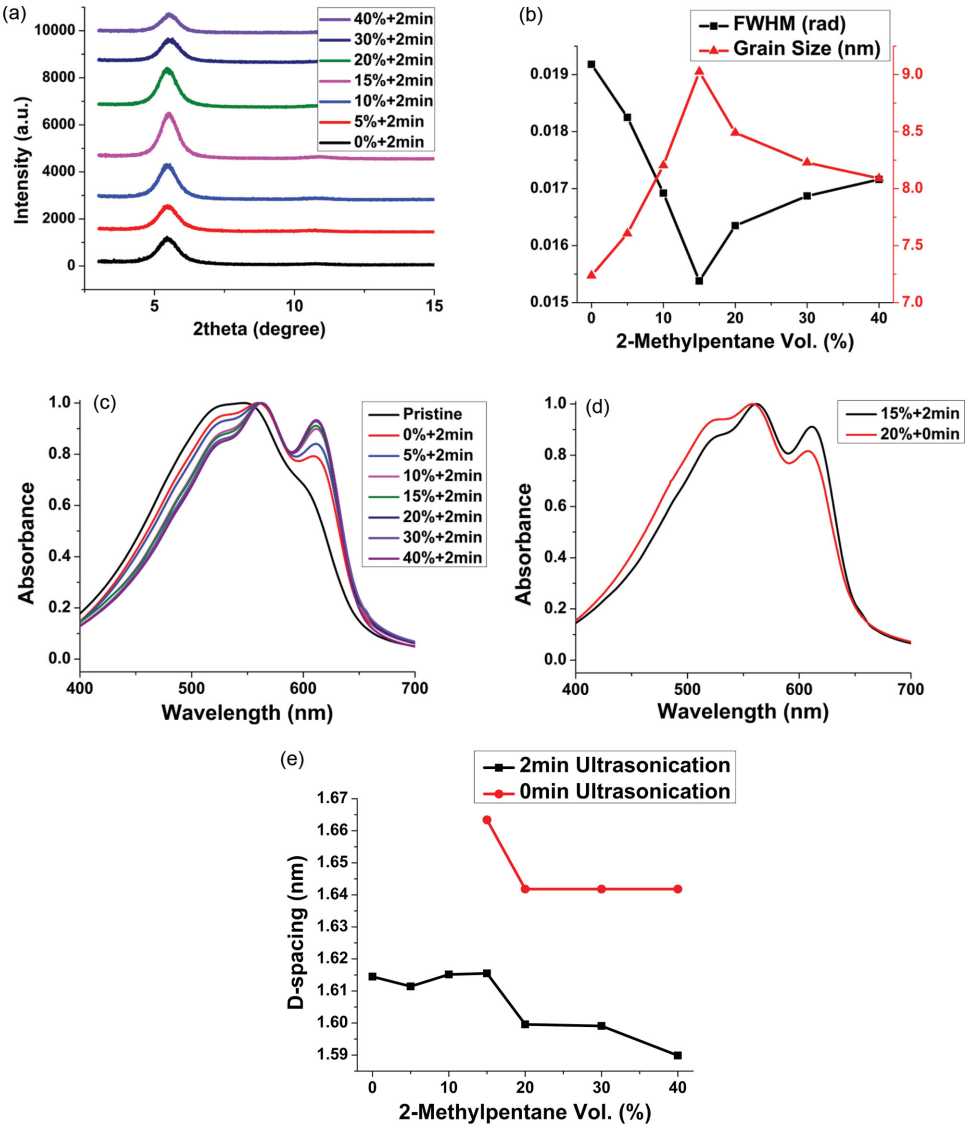

Figure 3. a) In-plane grazing incidence X-ray diffraction measurements for P3HT thin films fabricated from chloroform-P3HT solutions with varied proportions of 2-methylpentane and a fixed 2 min ultrasonication time. b) FWHM values of corresponding GIXRD profiles and calculated crystallite size. c,d) Normalized UV–vis absorption spectra of films fabricated from chloroform-P3HT solution c) with varied proportion of nonsolvent (2-methylpentane) treated by ultrasonication for 2 min and d) with 15 vol% 2-methylpentane treated by 2 min ultrasonication and with 20 vol% 2-methylpentane. e) (100) d-spacing values as a function of 2-methylpetane vol% (fixed 2 min ultrasonication time and without ultrasonication) calculated from corresponding GIXRD data.

of more nucleation sites (seeds). Both are in same degree of supersaturation; however, they differ in their respective fraction of nucleation sites. Applying the nucleation-growth model, formation of fewer yet longer nanorods is expected in system A versus system B. Alternatively, systems C and D have the same number of nucleation sites but different quantities of available P3HT. As a result, longer P3HT nanorods are expected to be assembled in system D.

The effects of nonsolvent and ultrasonication must first be articulated separately. The AFM phase images of P3HT thin films fabricated from solutions with varying proportions of 2-methylpentane (Figure 4a) demonstrate the role and impact of nonsolvent addition on P3HT nanorod formation. For up to 15 vol% 2-methylpentane, there is obvious growth of P3HT nanorod assemblies reaching 760 nm in length with a gradual increase in the number of features from none to 15 counts, following anticipated crystallization behavior in the metastable zone where growth and nucleation are favored and suppressed, respectively. Increasing the nonsolvent volume fraction above 15 vol% resulted in formation of an abruptly larger number of P3HT nanorods with shorter length, indicating domination of nucleation over growth. Transition from 15% to 20% provokes steep increase in number of nanorod assembly from 15 to 176 counts accompanying decrease in length from 760 to 400 nm. In this region, the P3HT solution falls into the unstable region where excessive nucleation takes place, thus a large number of small features are formed, as per the example scenario of systems A versus B (Figure 5d).

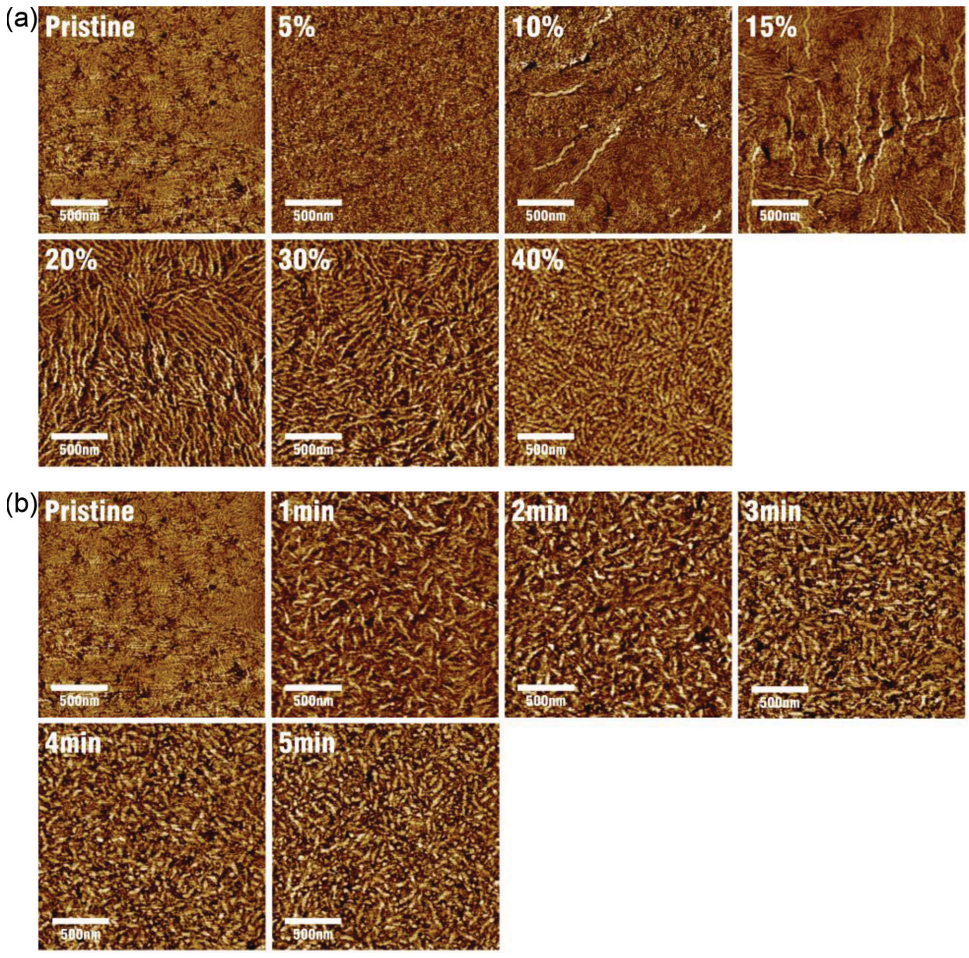

Figure 4. Tapping mode AFM phase images of P3HT thin films a) prepared via spin coating from $CHCl_3$ solution with defined proportions of 2-methylpentane and b) prepared via spin coating from $CHCl_3$ solution after ultrasonication for the indicated times.

Ultrasonication of a solution effects cavitation due to rapid expansion and compression of the liquid molecules in a process induced by the applied acoustic waves.[41,42] Microbubbles form and grow as the expansion and compression cycles are repeated, and finally collapse. When the microbubbles rupture, the surrounding liquid molecules near the microbubble wall experience very high pressure, which forces a localized portion of liquid near the microbubble to become highly supersaturated. As a result of this localized increased degree of supersaturation, nucleation sites are formed.[41–46] Examination of AFM phase images of P3HT thin films fabricated from chloroform solution with varied ultrasonication time (Figure 4b), confirms this phenomenon. As ultrasonication time increases, the number of small nanorods gradually increases as a result of an increased number of nucleation sites. Within 2 μm × 2 μm AFM image, nanorods count grows from 178 to 350 when ultrasonication time varies from 1 to 5 min. The size of nanorods fabricated via ultrasonication is relatively small, because without poor solvent mediation, the pristine P3HT-chloroform solution does not have a high degree of supersaturation and availability of excess solute is insufficient for further growth. Thus, through ultrasonic irradiation, the formation of nucleation sites for P3HT nanorod assembly can be promoted and controlled. On the contrary, 2-methylpentane addition provides a means to control the degree of supersaturation. Solubility modulation within the metastable zone stimulates nanorod growth, while extreme modulation of solubility forces the solution into the unstable regime and triggers spontaneous nucleation.

The 2-step crystallization model can be applied to P3HT self-assembly via sequential nonsolvent addition and ultrasonication by revisiting Figure 2a. Ultrasonication of P3HT-chloroform for 1–3 min promotes a degree of nucleation that is well balanced for subsequent growth. However, P3HT in pristine chloroform solution is in a low degree of supersaturation, and the conjugated polymer experiences only limited growth into small nanostructured assemblies (Figure 4b). As the degree of supersaturation is modulated through 2-methylpentane addition, nanostructure growth is enhanced and significantly longer assemblies are formed, exactly resembling the system C versus D scenario (Figure 5d). Above 15% nonsolvent, the solution experiences an increased degree of supersaturation which exceeds that desired for the metastable state, and nucleation dominates growth (Figure 5c). As a result, large quantities of shorter P3HT nanorods are formed (Figure 4a). Ultrasonication of solutions that have been excessively driven into supersaturation leads to even more extensive nucleation. For instance,

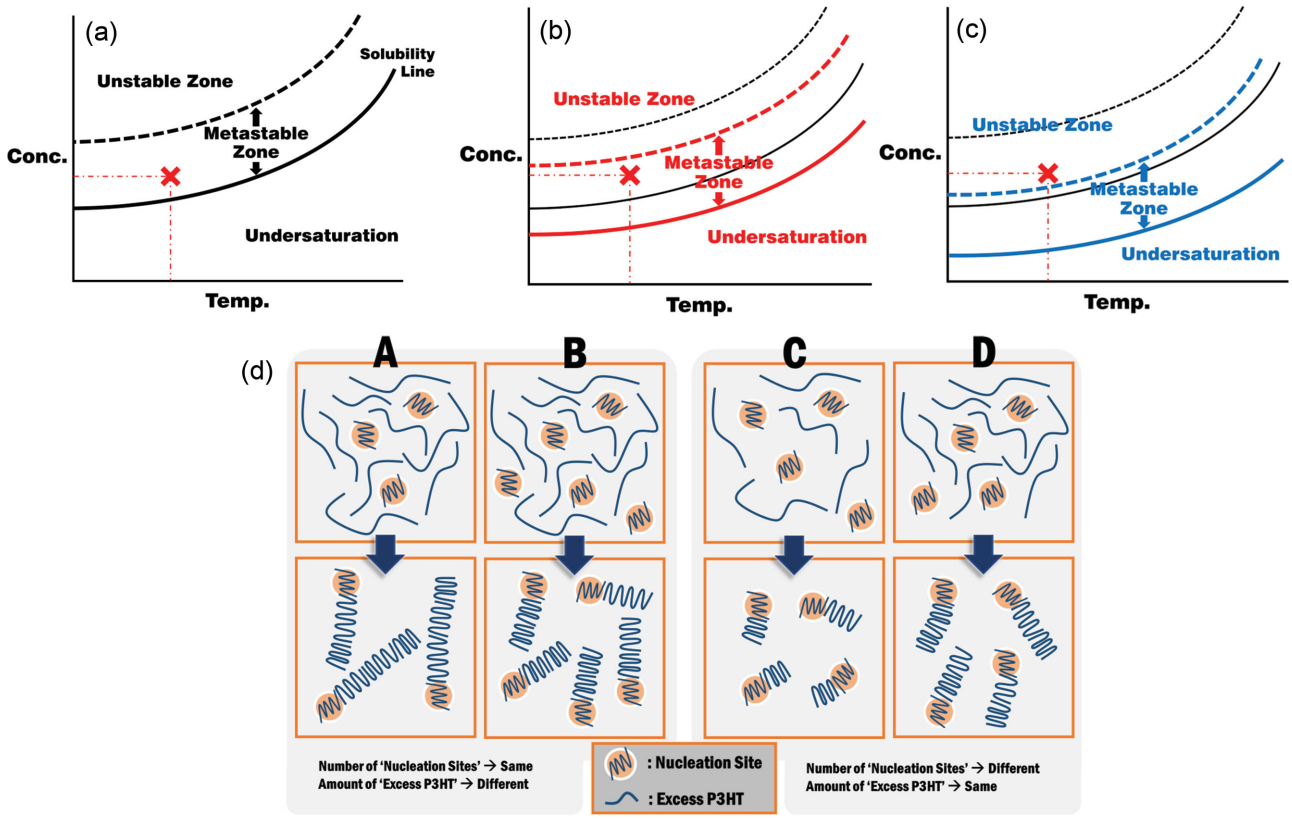

Figure 5. a–c) Typical solubility curves depicting the metastable and unstable zone. The red X indicates a fixed value of solution temperature and concentration. a) Black lines represent the solubility curve for the solution under the initial moderately supersaturated conditions. b) The solubility curve of the solution after poor solvent addition is given in red lines. The red X resides in metastable zone. c) Further addition of poor solvent leads to conditions depicted with blue lines where the solution condition marked by red X enters the unstable zone. d) Schematic depicting four general cases of P3HT self-assembly based on the 2-step crystallization model.

note that P3HT solutions with 30 and 40 vol% 2-methylpentane produce thin films with nanorods having average length of 310 and 240 nm, respectively, which are far shorter than those of 15 vol% 2-methylpentane sample consisting 760-nm-length nanorods (Figure 4a); ultrasonication of solutions in unstable state for 2 min results in films composed of even shorter P3HT assemblies (Figure 2a).

An experimental protocol was designed to confirm the validity of the 2-step crystallization model for P3HT self-assembly. Specifically, the volume fraction of 2-methylpentane was maintained at 15%, while ultrasonication time was varied from 1 to 3 min. This approach controlled the degree of supersaturation, and thus the 2-step crystallization model predicts the formation of shorter nanorods when ultrasound is applied for longer times, simply because ultrasonication stimulates nucleation site formation. The experimental results exactly followed these expectations. **Figure 6** depicts AFM images of P3HT thin films prepared from the solvent blend as a function of sonication time. With increased sonication time, length of assembled polymer nanorods decreased from 420 to 210 nm. As shown in Figure 4b, the number of nucleation sites gradually increases with increased ultrasonication time. Thus, with a fixed proportion of 2-methylpentane, the length of the nanorod assemblies should shorten as the amount of excess P3HT available for growth from each nucleation site decreases.

Through systematic study and analysis of the AFM morphological images, verification that the assembly process of P3HT into nanorod structures follows a 2-step crystallization model was obtained. Moreover, the individual contributions of ultrasonication and nonsolvent addition, specifically 2-methylpentane, on P3HT nanorod formation were elucidated.

3. Conclusion

Synergistic use of solubility modulation and ultrasonication, facilitates the controlled assembly of highly ordered P3HT nanostructures, where the length of rod-like assemblies could be systematically modulated. P3HT thin films comprised of nanorod structures assembled in solution through the synergistic approach exhibited hole mobilities reaching an average of 0.103 $cm^2 V^{-1} s^{-1}$ versus only 0.025 $cm^2 V^{-1} s^{-1}$ for the untreated counterparts. Analysis of the results suggests a new processing methodology for enhanced electronic performance, and importantly allows mechanistic interpretation of P3HT self-assembly. The simple yet powerful 2-step crystallization model consisting of nucleation and growth steps was applied, for the first time, to describe P3HT self-assembly. Arrays of experimental results confirmed the validity of the 2-step crystallization approach to understanding self-assembly processes of the conjugated

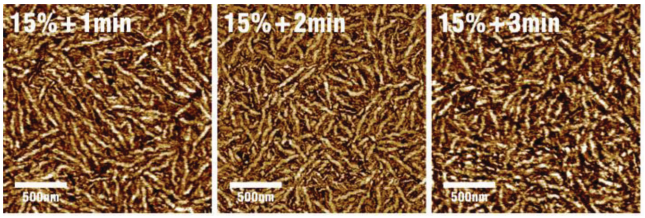

Figure 6. AFM phase images of P3HT thin films prepared via spin coating from $CHCl_3$/2-methylpentane (85/15 v/v) solution with the defined ultrasonication time.

polymer into mesoscale entities. Length and density of self-assembled rod-like P3HT nanostructures created in solution through nonsolvent addition, ultrasonication, and sequential combination of both treatments exactly followed model predictions. Modulation of solution solubility informs optimal/favorable solution conditions for nanostructure growth, while ultrasonication plays a significant role in creating nucleation sites. Moreover, experimental protocols fixing solution solubility but varying ultrasonication time were designed to validate the proposed mechanistic model.

The experimental results were in agreement with the predictions, further supporting the model as a straight forward, yet powerful platform to provide new insights into conjugated polymer self-assembly into mesoscale structures. Systematic analysis of AFM images, GIXRD, UV–vis, and mobility data highlights the existence and significance of interplay between long-range ordering and molecular level interactions for efficient charge carrier transport. Long-range order, as discerned from conjugated polymer nanorod length, is a necessary but insufficient requirement. The importance of molecular level interactions for effective macroscopic charge carrier transport was also elucidated. However, in the absence of adequate structures of a critical length, the degree of long-range order becomes dominant. The insights provided here will substantially impact the design and development of solution-based conjugated polymer processes for flexible electronic and photonic applications.

4. Experimental Section

Materials: P3HT was purchased from Reike Metals Inc. and used without further purification. The P3HT used in this study had a M_w of 90 kDa, polydispersity of 2.3, and 96% regioregularity. Since it has been widely reported that higher molecular weight P3HT exhibits higher charge carrier mobility among commercially available 96% regioregular P3HT from Reike Metals Inc., 90 kDa P3HT has been selected. Chloroform (Anhydrous) and 2-methylpentane (Anhydrous) were purchased from Sigma-Aldrich.

Controlled Assembly of P3HT Nanorods in Solution: A combination of 2-methylpentane addition and ultrasonication was used to fabricate P3HT nanorods in solution. First, a chloroform-P3HT solution was prepared: 10 mg of P3HT was introduced into 2 mL of chloroform in a 20-mL borosilicate glass vial. The vial was capped and placed on top of a hot plate at ≈55 °C for 30 min to ensure complete dissolution of P3HT. After the complete dissolution of P3HT, the solution was allowed to cool to room temperature. Then, the designated amount of 2-methylpentane was slowly added to the chloroform-P3HT solution. The as-prepared solution was then ultrasonicated for the specified time using a tabletop bath-type ultrasonicator (Bransonic 2510, 40 kHz, 130 W) filled with tap water. The dissolution and ultrasonication processes were performed in air.

Organic Field-Effect Transistor (OFET) Fabrication and Characterization: The OFET devices with bottom-gate, bottom-contact structure were fabricated to perform electrical characterization of P3HT films fabricated from solutions prepared as above. Highly n-doped silicon wafers with a thermally grown 300-nm-thick SiO_2 dielectric surface were used as the substrate. The highly doped silicon substrate served as the gate electrode with the thermally grown SiO_2 as the dielectric layer. Au/Cr was used for the source and drain contacts. The source and drain contacts were fabricated using a standard photolithography based lift-off process inside a cleanroom, followed by E-beam evaporation (Denton Explorer) of 50 nm Au contacts with 3 nm of Cr as the adhesion layer. Before spin-coating P3HT solutions, all devices were cleaned for 30 min in a UV-ozone cleaner (Novascan PSD-UV) to completely remove any residual photoresist and other organic contaminants. OFET devices were prepared by spin-coating (WS-650MZ-23NPP, Laurell) the solutions onto precleaned devices at a spin speed of 1500 rpm for 60 s in air, and tested in nitrogen ambient using an Agilent 4155C semiconductor parameter analyzer. The devices were stored in a vacuum oven (1 Torr) overnight at 50 °C to remove residual solvent. The field-effect hole mobility was calculated in the saturation regime of transistor operation ($V_D = -3$ V) by plotting the drain current (I_D) versus gate voltage (V_G) and fitting the data to the following equation

$$I_D = \mu C_{ox} \frac{W}{L}(V_G - V_T)V_D$$

where W (2000 μm) and L (50 μm) are the transistor channel width and length, respectively, V_T is the threshold voltage, and C_{OX} is the capacitance per unit area of the silicon dioxide gate dielectric (1.15×10^{-8} F cm^{-2}). For each condition, five OFET devices were fabricated and tested for calculation of average mobility.

UV–Vis Spectra of P3HT: The solid state UV–vis spectra were obtained using an Agilent 8510 Spectrophotometer. Corresponding P3HT films were spin coated onto precleaned glass slides.

Grazing Incidence X-Ray Diffraction (GIXRD): Out-of-plane grazing incidence X-ray diffraction data were obtained using a Panalytical X'Pert Pro system equipped with a Cu X-ray source operating at 45 kV and 40 mA. Grazing incidence angle was fixed at 0.2° and the detector was scanned from 3° to 30°. Samples for GIXRD measurements were prepared by spin coating corresponding P3HT solutions on sliced n-doped silicon wafer with 300 nm thermally grown SiO_2, identical to that used for fabricating OFET substrates. Substrates were cleaned using the same procedure used for OFET devices.

Atomic Force Microscopy (AFM): The AFM measurements were performed on the area between the source and drain channels of OFET devices after finishing electrical performance measurements of the corresponding devices. The Dimension Icon atomic force microscope (Bruker) operated in tapping mode with a silicon tip (NCS-14, Mikromasch) was used for all AFM measurements.

Supporting Information

Supporting Information is available from the Wiley Online Library or from the author.

Acknowledgements

The financial support of the Georgia Institute of Technology and the National Science Foundation (CBET 1264555) is gratefully acknowledged. The authors would also like to thank Ping-Hsun Chu and Nils Perssons at the Georgia Institute of Technology for their helpful discussions.

Received: October 22, 2014
Revised: November 24, 2014
Published online: December 18, 2014

[1] H. Sirringhaus, *Adv. Mater.* **2014**, *26*, 1319.
[2] Y. Huang, E. J. Kramer, A. J. Heeger, G. C. Bazan, *Chem. Rev.* **2014**.
[3] H. Klauk, *Chem. Soc. Rev.* **2010**, *39*, 2643.
[4] H. Sirringhaus, *Adv. Mater.* **2005**, *17*, 2411.
[5] Y.-J. Cheng, S.-H. Yang, C.-S. Hsu, *Chem. Rev.* **2009**, *109*, 5868.
[6] C. Wang, H. Dong, W. Hu, Y. Liu, D. Zhu, *Chem. Rev.* **2012**, *112*, 2208.
[7] W. Wu, Y. Liu, D. Zhu, *Chem. Soc. Rev.* **2010**, *39*, 1489.
[8] Y. Mei, M. A. Loth, M. Payne, W. Zhang, J. Smith, C. S. Day, S. R. Parkin, M. Heeney, I. McCulloch, T. D. Anthopoulos, J. E. Anthony, O. D. Jurchescu, *Adv. Mater.* **2013**, *25*, 4352.
[9] P. J. Diemer, C. R. Lyle, Y. Mei, C. Sutton, M. M. Payne, J. E. Anthony, V. Coropceanu, J.-L. Brédas, O. D. Jurchescu, *Adv. Mater.* **2013**, *25*, 6956.
[10] Y. Diao, B. C.-K. Tee, G. Giri, J. Xu, D. H. Kim, H. A. Becerril, R. M. Stoltenberg, T. H. Lee, G. Xue, S. C. B. Mannsfeld, Z. Bao, *Nat. Mater.* **2013**, *12*, 665.
[11] G. Giri, E. Verploegen, S. C. B. Mannsfeld, S. Atahan-Evrenk, D. H. Kim, S. Y. Lee, H. A. Becerril, A. Aspuru-Guzik, M. F. Toney, Z. Bao, *Nature* **2011**, *480*, 504.
[12] H. Li, B. C.-K. Tee, G. Giri, J. W. Chung, S. Y. Lee, Z. Bao, *Adv. Mater.* **2012**, *24*, 2588.
[13] Y. Wen, Y. Liu, Y. Guo, G. Yu, W. Hu, *Chem. Rev.* **2011**, *111*, 3358.
[14] M. Mas-Torrent, C. Rovira, *Chem. Rev.* **2011**, *111*, 4833.
[15] N. D. Treat, J. A. N. Malik, O. Reid, L. Yu, C. G. Shuttle, G. Rumbles, C. J. Hawker, M. L. Chabinyc, P. Smith, N. Stingelin, *Nat. Mater.* **2013**, *12*, 628.
[16] C. Luo, A. K. K. Kyaw, L. A. Perez, S. Patel, M. Wang, B. Grimm, G. C. Bazan, E. J. Kramer, A. J. Heeger, *Nano Lett.* **2014**, *14*, 2764.
[17] H.-R. Tseng, H. Phan, C. Luo, M. Wang, L. A. Perez, S. N. Patel, L. Ying, E. J. Kramer, T.-Q. Nguyen, G. C. Bazan, A. J. Heeger, *Adv. Mater.* **2014**, *26*, 2993.
[18] A. R. Aiyar, J.-I. Hong, R. Nambiar, D. M. Collard, E. Reichmanis, *Adv. Funct. Mater.* **2011**, *21*, 2652.
[19] Y. D. Park, H. S. Lee, Y. J. Choi, D. Kwak, J. H. Cho, S. Lee, K. Cho, *Adv. Funct. Mater.* **2009**, *19*, 1200.
[20] J. J. De Yoreo, *Rev. Mineral. Geochem.* **2003**, *54*, 57.
[21] P. G. Vekilov, *Cryst. Growth Des.* **2010**, *10*, 5007.
[22] B. H. Ryu, J. Ulrich, *Cryst. Growth Des.* **2012**, *12*, 6126.
[23] D. Erdemir, A. Y. Lee, A. S. Myerson, *Acc. Chem. Res.* **2009**, *42*, 621.
[24] J.-F. Chang, B. Sun, D. W. Breiby, M. M. Nielsen, T. I. Sölling, M. Giles, I. McCulloch, H. Sirringhaus, *Chem. Mater.* **2004**, *16*, 4772.
[25] A. R. Aiyar, J.-I. Hong, J. Izumi, D. Choi, N. Kleinhenz, E. Reichmanis, *ACS Appl. Mater. Interfaces* **2013**, *5*, 2368.
[26] T. W. Kelley, C. D. Frisbie, *J. Phys. Chem. B* **2001**, *105*, 4538.
[27] J. Rivnay, L. H. Jimison, J. E. Northrup, M. F. Toney, R. Noriega, S. Lu, T. J. Marks, A. Facchetti, A. Salleo, *Nat. Mater.* **2009**, *8*, 952.
[28] R. Street, J. Northrup, A. Salleo, *Phys. Rev. B* **2005**, *71*, 165202.
[29] U. Holzwarth, N. Gibson, *Nat. Nanotechnol.* **2011**, *6*, 534.
[30] M. Chang, D. Choi, B. Fu, E. Reichmanis, *ACS Nano* **2013**, 5402.
[31] G. Nagarjuna, M. Baghgar, J. A. Labastide, D. D. Algaier, M. D. Barnes, D. Venkataraman, *ACS Nano* **2012**, *6*, 10750.
[32] M. J. Winokur, D. Spiegel, Y. Kim, S. Hotta, A. J. Heeger, *Synth. Met.* **1989**, *28*, 419.
[33] J. Clark, C. Silva, R. Friend, F. Spano, *Phys. Rev. Lett.* **2007**, *98*, 206406.
[34] M. Chang, J. Lee, N. Kleinhenz, B. Fu, E. Reichmanis, *Adv. Funct. Mater.* **2014**.
[35] J. Huang, M. Kertesz, *J. Chem. Phys.* **2005**, *122*, 234707.
[36] A. Troisi, G. Orlandi, *J. Phys. Chem. A* **2006**, *110*, 4065.
[37] H. Yamagata, C. M. Pochas, F. C. Spano, *J. Phys. Chem. B* **2012**, *116*, 14494.
[38] J. B. Rawlings, S. M. Miller, W. R. Witkowski, *Ind. Eng. Chem. Res.* **1993**, *32*, 1275.
[39] P. Cubillas, M. W. Anderson, in *Zeolites and Catalysis*, Wiley-VCH Verlag GmbH & Co. KGaA, Weinheim, Germany **2010**, pp 1–55.
[40] M. Muthukumar, in *Advances in Chemical Physics*, Vol. *128*, John Wiley & Sons, Inc., Hoboken, NJ, USA **2004**.
[41] R. Hickling, *J. Acoust. Soc. Am.* **1994**, *73*, 2853.
[42] X. Zhang, T. Inada, A. Tezuka, *Ultrason. Sonochem.* **2003**, *10*, 71.
[43] D. W. Oxtoby, *Acc. Chem. Res.* **1998**, *31*, 91.
[44] R. P. Frydenberg, M. Hammershøj, U. Andersen, L. Wiking, *Cryst. Growth Des.* **2013**, *13*, 5375.
[45] B. C. Knott, J. L. LaRue, A. M. Wodtke, M. F. Doherty, B. Peters, *J. Chem. Phys.* **2011**, *134*, 171102.
[46] A. Kordylla, T. Krawczyk, F. Tumakaka, G. Schembecker, *Chem. Eng. Sci.* **2009**, *64*, 1635.